RSC Advances

ROYAL SOCIETY OF CHEMISTRY

www.rsc.org/advances

RSC Advances

PAPER

# Improved High-temperature Hydrothermal Stability of Cu-SSZ-13 by an Ammonium Hexafluorosilicate Treatment

Received 00th January 20xx,
Accepted 00th January 20xx

DOI: 10.1039/x0xx00000x

**www.rsc.org/**

Yu Zhang [a], Hongning Wang [a] and Ruoyu Chen [a] *

The hydrothermal stability of selective catalytic reduction (SCR) catalysts is a critical factor in the design of an after-treatment system for diesel engine exhaust. In the present study, Cu-SSZ-13 catalysts were treated with ammonium hexafluorosilicate (AHFS) to improve their hydrothermal stability. Modified and unmodified Cu-SSZ-13 catalysts were then hydrothermally aged at 850 °C in a simulated exhaust gas containing water for 6 and 12 h. Their catalytic activities were tested in a fixed-bed reactor system. X-ray diffraction (XRD), transmission electron microscopy (TEM), $N_2$-adsorption, inductively coupled plasma-auger electron spectroscopy (ICPAES), $^{27}$Al and $^{29}$Si solid state nuclear magnetic resonance (NMR), vacuum fourier transform infrared spectroscopy (FT-IR), and Raman spectroscopy were employed to elucidate the effects of AHFS treatment. The results showed that the modified Cu-SSZ-13 catalyst maintained its high SCR activity after hydrothermal aging whereas the unmodified Cu-SSZ-13 catalyst exhibited remarkably lower NO conversions at all temperatures tested. The results consistently indicated that the chabazite (CHA) structure of the modified Cu-SSZ-13 catalyst was preserved after hydrothermal aging whereas the CHA structure of unmodified Cu-SSZ-13 collapsed. The observed collapse of the CHA structure of the unmodified Cu-SSZ-13 catalyst was determined to be the result of dealumination of the $Si(OSi)_2(OAl)_2$ and $Si(OSi)_3(OAl)$ structures during hydrothermal aging. Moreover, the copper ions were converted into CuO particles. However, AHFS treatment induced the $Si(OSi)_2(OAl)_2$ structure to transform into the $Si(OSi)_3(OAl)$ and $Si(OSi)_4$ structures with better hydrothermal stabilities, which better maintained the CHA structure after high temperature hydrothermal aging. Meanwhile, the $OH^-$ ions of the surface Si-OH groups could be exchanged with $F^-$ ions to form a highly stable hydrophobic surface, which prevented steam from eroding the Cu-SSZ-13 catalyst.

## 1. Introduction

Great interest has been recently generated in the more widespread use of lean burn diesel engines due to better fuel economy and greater power density relative to conventional gasoline engines.[1] However, to meet emission standards, their use depends on the effective reduction of two primary diesel exhaust components: nitrogen oxides ($NO_x$) and particulate matter (PM).[2] The selective catalytic reduction of $NO_x$ by $NH_3$ ($NH_3$-SCR) is a commercially proven technology for removing $NO_x$ from diesel engine exhaust.[3,4] A typical $NH_3$-SCR after-treatment system includes a diesel particulate filter (DPF). The DPF must be periodically heated to high temperatures (> 650 °C) to burn off the trapped PM and a great deal of heat might then be transferred to the SCR catalyst. High-temperature exposure in the presence of moisture in the feed can damage the zeolite framework of the SCR catalyst, resulting in deactivation. Therefore, resistance to hydrothermal aging can be crucial for $NH_3$-SCR catalyst applications.

Cu-exchanged zeolites have been increasingly studied as SCR catalyst materials following the pioneering work of Iwamoto and Hamada on Cu-ZSM-5.[5] M. Moliner et al. found Cu-SSZ-39 which cages are similar in size to CHA cages was an active and stable catalyst for the selective catalytic reduction of $NO_x$.[6] However, most Cu-zeolite catalysts lack the hydrothermal stability required to function within diesel exhaust treatment systems.[7-11] A major breakthrough was achieved in 2009 when researchers from BASF Corp. and Johnson Matthey Inc. discovered that Cu-exchanged chabazite (such as Cu-SSZ-13) catalysts offer both hydrothermal stability and low/high-temperature reactivity for commercial applications.[10] Xie et al. designed a one-pot synthesis method of Cu-SSZ-13 catalyst using low-cost copper-tetraethylenepentamine (Cu-TEPA) as a novel template, which has excellent performance for the selective catalytic reduction of $NO_x$ with $NH_3$.[12] The SSZ-13 zeolites have the largest pore opening of 0.38 nm, and transport of the dealumination product, $Al(OH)_3$, which has a kinetic diameter of 0.50 nm, is likely to be restrained by the small pores. As a result, the dealumination process is hindered during hydrothermal aging.[13] In the past several years, Cu-SSZ-13 catalysts have been implemented as SCR catalysts for diesel vehicles. Nevertheless, these catalysts require improved hydrothermal stability to accommodate applications in higher-temperature environments. As an example, Schmieg et al. recently found that hydrothermal aging of the Cu-SSZ-13 catalyst at 850 °C for 12 h resulted in a

---

[a] School of Petrochemical Engineering, Changzhou University, 1 Gehu Road, Changzhou, Jiangsu 213164, PR China. E-mail address: cxdcry@163.com

significantly reduced SCR performance. This was accompanied by a drastic loss in crystallinity and a greatly reduced number of active Cu sites.[14] Kim et al. found that $Cu^{2+}$ ions on the Cu-SSZ-13 have different hydrothermal stabilities. Particularly, $Cu^{2+}$ ions in the CHA cage were found to be less stable than the $Cu^{2+}$ ions in the D6R unit, therefore, the authors believed the former structure is primarily responsible for the hydrothermal aging of Cu-SSZ-13 catalysts. Therefore, it is necessary to further improve the high-temperature hydrothermal stability of the Cu-SSZ-13 catalyst.[15]

Ammonium fluorosilicate (AHFS) is a commonly used reagent in the dealumination of H-Y and H-ZSM-5 zeolites that repairs the defects in the zeolite crystal by incorporating silicon into the microporous framework, which stabilizes the zeolite during dealumination.[16,17] In the present study, Cu-SSZ-13 catalysts were treated with AHFS solution to improve their hydrothermal stability. We employed XRD, TEM, $N_2$ absorption, NMR, ICPAES, FT-IR, and Raman spectroscopy to characterize the structure, Cu species, and the SCR activities of the Cu-SSZ-13 catalyst during hydrothermal treatment.

## 2. Experimental

### 2.1 Catalyst preparation

The SSZ-13 zeolite was synthesized as previously reported by Zones et al.[18] Briefly stated, 1.3 g of aluminum sulfate (> 99%, Sinopharm), 0.95 g of NaOH (> 96%, Sinopharm), 16.4 g of N,N,N-trimethyl-1-adamantanamine hydroxide (25 wt%, Zhongbangst), and 9 ml of deionized (DI) water were stirred for 30 min at 20 °C. Then, 16 g of silica solution (30 wt%, Sigma-Aldrich) was added to the solution and mixed for 2 h. After mixing, the sample was transferred to a stainless steel autoclave with a Teflon liner, which was heated at 155 °C for 3 days in a convection oven. The resulting product was washed by DI water and dried at 100 °C overnight in air.

The obtained Na-SSZ-13 zeolite was added to a 0.5 M solution of ammonium nitrate with continuous stirring at 80 °C for 8 h. The resulting material was washed and dried at 100 °C overnight to obtain $NH_4$-SSZ-13. The $NH_4$-SSZ-13 sample was calcined at 550 °C for 6 h to obtain H-SSZ-13. Next, the sample was ion exchanged with 0.05 M $Cu(CH_3COO)_2$ at 40 °C for 24 h. The Cu-exchanged sample was filtered, washed with DI water, dried at 100 °C overnight to obtain Cu-SSZ-13.

The Cu-SSZ-13 sample (3 g) was dispersed in 100 mL of 0.01 M AHFS solution with stirring at 60 °C for 0.5 h, 1 h, 2 h, or 4 h. Next, the filtered solid was washed twice and dried at 100 °C for 4 h. Finally, the catalysts were calcined at 550 °C for 5 h. The AHFS-treated Cu-SSZ-13 samples are identified as Cu-S-*X*, where *X* denotes the AHFS-treatment time (h).

### 2.2 Catalyst characterization

The XRD patterns were collected on a Rigaku D/MAX2500 diffractometer with a Cu $K_\alpha$ radiation source ($\lambda$ = 0.154056 nm), a tube voltage of 40 kV, and a tube current of 100 mA. The scanning rate was 3° per min within a $2\theta$ value of 5–50°. The TEM images were performed on a JEOL JEM-2100 transmission electron microscope operating at 200 kV. For the TEM measurements, the samples were dispersed in ethanol and then dried on a holey carbon film Cu grid. The pore structure of the catalysts were measured with a Micrometritics ASAP 2020 physical adsorption instrument at −196 °C. The micropore volume was calculated according to a t-plot method, and the average micropore diameter was calculated using the Horvath-Kawazoe (HK) method. Solid state $^{27}Al$ and $^{29}Si$ NMR spectra were obtained on a Bruker AVANCE III 500 MHz instrument. The $^{27}Al$ magic angle spinning (MAS) NMR spectra were recorded at a resonance frequency of 130.3 MHz, and $^{29}Si$ MAS NMR spectra were recorded at a resonance frequency of 99.4 MHz. The $^{27}Al$ chemical shifts, given in parts per million (ppm), were reported relative to a 0.1 M aqueous $Al(NO_3)_3$ solution and the $^{29}Si$ chemical shifts (ppm) were referenced to a $Si(CH_3)_4$. The elemental compositions of the samples were analyzed by ICPAES (Varian Vista-AX, America). Vacuum FTIR spectra were collected with a Bruker Vertex 80V Vacuum Fourier infrared Spectrometer. Each spectrum was recorded from 400 $cm^{-1}$ to 4000 $cm^{-1}$ with a resolution of 2$cm^{-1}$. The Raman spectra were collected on a Thermo Fisher DXR spectrometer.

### 2.3 Catalyst activity tests

Catalytic activity was tested in a fixed-bed quartz tube reactor. A catalyst sample (1.5 g; 80–120 mesh size powder) was loaded in a quartz tube that was placed inside a tube furnace. The simulated exhaust gas was comprised of 600 ppm NO, 600 ppm $NH_3$, 5% $H_2O$

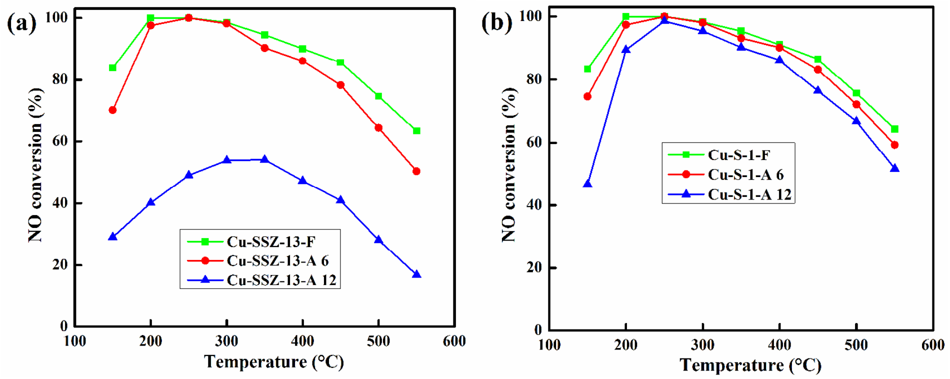

**Fig. 1** SCR performance for Cu-SSZ-13 (a) and Cu-S-1 (b) before and after 850 °C hydrothermal aging for 6 h and 12 h.

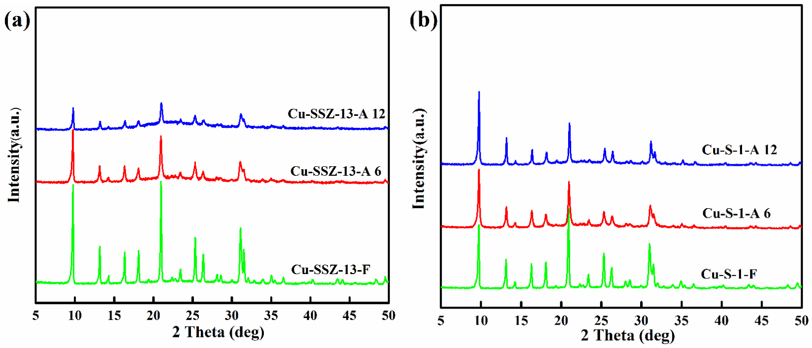

**Fig. 2** XRD patterns of Cu-SSZ-13 (a) and Cu-S-1 (b) before and after 850 °C hydrothermal aging for 6 h and 12 h.

and 8% $O_2$ in an $N_2$ background, and the gas hourly space velocity (GHSV) was 30,000 $h^{-1}$. Catalyst activity tests were investigated from 150–550 °C. Gas compositions before and after reaction were analyzed on-line with Kane-9106E flue gas analyser. The $NO_x$ conversion $\eta$ was calculated by the following equation:

$$\eta = ((C_1 - C_0)/C_1) \times 100\%,$$

where $C_1$ and $C_0$ are the concentrations of $NO_x$ before and after the reaction, respectively.

Hydrothermal aging was performed in the presence of 5% $H_2O$ and 20% $O_2$ with the remainder being $N_2$ at a GHSV of 30,000 $h^{-1}$. Both AHFS-treated and untreated catalysts were progressively aged at 850 °C for 6 h and 12 h, respectively. The SCR activities of aged catalysts were tested according to the method described above.

## 3. Results and discussion

### 3.1. SCR performance

The SCR performance data for the untreated Cu-SSZ-13 and AHFS-treated Cu-S-1 catalysts before and after hydrothermal aging for 6 and 12 h are shown in Fig. 1, respectively. Both catalysts exhibited good initial SCR activities over the range of temperatures considered, and the NO conversion trends were essentially identical. In particular, over 98% NO conversion was achieved at temperatures between 200 and 350 °C for both catalysts. After hydrothermal aging for 6 h, the SCR activities at low-temperatures (< 200 °C) and temperatures above 400 °C were slightly reduced for both the untreated Cu-SSZ-13 and Cu-S-1 catalysts, although NO conversion at temperatures of 200 to 400 °C remained over 90%. Relative to the Cu-S-1 catalyst, the NO conversion of the untreated Cu-SSZ-13 catalyst aged for 6 h decreased more obviously, where it was 50% at 550 °C, corresponding to a 13% reduction from that obtained with the initial catalyst (Fig. 1a). The NO conversion of the untreated Cu-SSZ-13 catalyst was significantly reduced over the test temperature range after

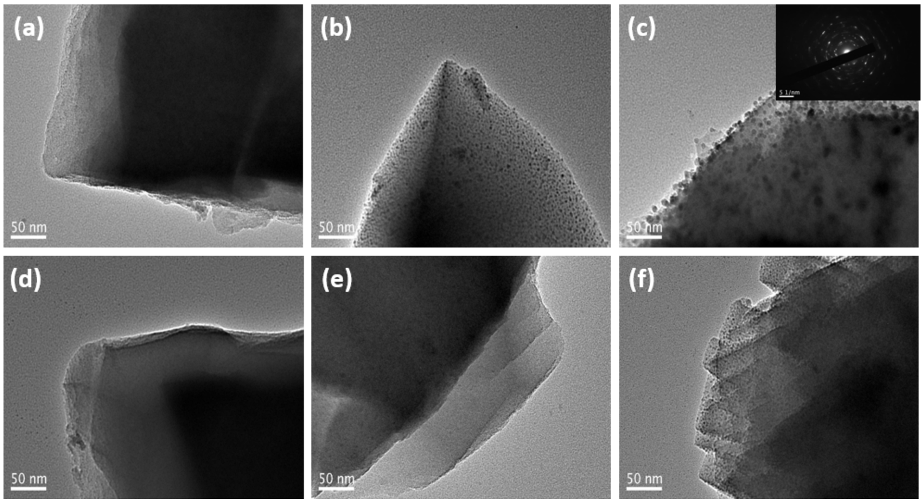

**Fig. 3** TEM images of different catalysts. (a) The original Cu-SSZ-13 catalyst; (b) Cu-SSZ-13 catalyst aged at 850 °C for 6 h; (c) Cu-SSZ-13 catalyst aged at 850 °C for 12 h; (d) The initial Cu-S-1 catalyst; (e) Cu-S-1 catalyst aged at 850 °C for 6 h; (f) Cu-S-1 catalyst aged at 850 °C for 12h

**Table.1** Physicochemical properties of Cu-SSZ-13 catalysts treated with different times.

| Sample | Cu (wt.%) | Si/Al | Micropore area ($m^2/g$)[a] | Pore size(nm)[b] |
|---|---|---|---|---|
| Cu-S-0.5(fresh) | 2.4 | 8.8 | 417 | 0.51 |
| Cu-S-1(fresh) | 2.2 | 8.8 | 391 | 0.51 |
| Cu-S-2(fresh) | 1.7 | 9.1 | 321 | 0.52 |
| Cu-S-4(fresh) | 1.0 | 9.7 | 189 | 0.54 |

a Determined by the *t*-plot approach.

b Calculated by the H-K model.

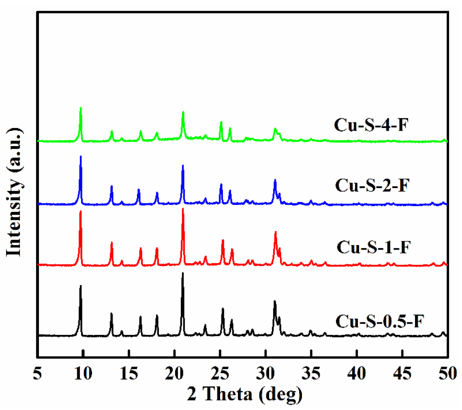

**Fig. 4** XRD patterns of Cu-SSZ-13 with different AHFS treatment time.

hydrothermal aging for 12 h, where a maximum NO conversion of 54% was observed at 350 °C. However, an NO conversion of greater than 90% was observed between 200 and 350 °C for the Cu-S-1 catalyst after aging for 12 h. The NO conversion at 550 °C suffered only a 13% reduction versus the initial Cu-S-1 catalyst (Fig. 1b). These findings indicate that AHFS treatment improved the hydrothermal stability of the Cu-SSZ-13 catalyst.

### 3.2 Characterization of the catalysts

XRD measurements were employed before and after hydrothermal treatment, as shown in Figs. 2, to examine the structural changes that occur during the hydrothermal aging of untreated Cu-SSZ-13 and AHFS-treated Cu-S-1 catalysts. As shown in Fig. 2b, the initial Cu-S-1 catalyst maintains the crystallinity of the original Cu-SSZ-13 after AHFS treatment, where all diffraction peaks related to the CHA phase are observed in the XRD pattern. After hydrothermal aging for 6 h, all diffraction peak intensities related to the CHA phase for the untreated Cu-SSZ-13 catalyst decreased slightly. The Cu-S-1 catalyst exhibited only a few diffraction peaks with diminished intensities. Hydrothermal aging for 12 h resulted in an even more dramatic collapse in the CHA crystal structure of the untreated Cu-SSZ-13 catalyst. On the other hand, very little change was observed for the aged Cu-S-1 catalyst, indicating that this zeolite structure was very well maintained during equivalent hydrothermal aging. This verifies that the Cu-S-1 structure was indeed more robust than that of the untreated Cu-SSZ-13 catalyst. The observed structural collapse of the untreated Cu-SSZ-13 structure occurring after hydrothermal aging corresponds to the dramatic drop in NO conversion observed during the SCR catalyst tests. While changes in the crystal structure of the catalysts with hydrothermal aging were readily apparent, the CuO peaks could not found in these XRD profiles.[19, 20]

The untreated Cu-SSZ-13 and Cu-S-1 catalysts before and after hydrothermal aging were characterized using TEM, as shown in Fig. 3. No visible particles were observed in the initial Cu-SSZ-13 and Cu-S-1 catalysts, which indicates that the Cu species were highly dispersed. The TEM image of the untreated catalyst aged for 6 h shows the presence of some black particles, which corresponds with the XRD results indicating a diminished zeolite structure. Electron diffraction indicated that these black particles are composed solely of CuO. However, the TEM image of the Cu-S-1 catalyst aged for 6 h exhibits no obvious changes relative to its initial state, indicating that the Cu species remained highly dispersed. When the aging time was increased to 12 h, the size of the black CuO particles observed in the untreated Cu-SSZ-13 catalyst increased by several nm. The Cu-S-1 also exhibited the presence of some black CuO particles whose general size was similar to that of the black particles observed in the untreated Cu-SSZ-13 catalyst aged for 6 h. We therefore conclude from the TEM

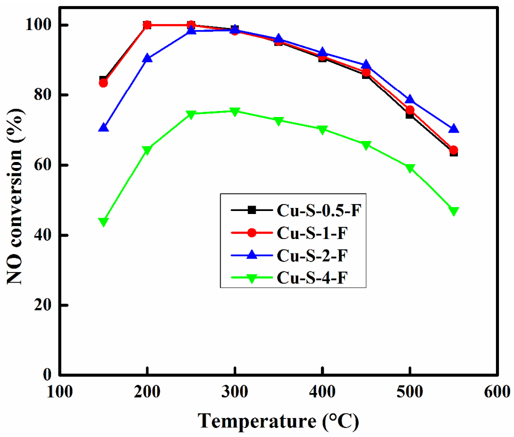

**Fig. 5** SCR performance for Cu-SSZ-13 catalysts with different AHFS treatment time.

**Table.2** Physicochemical properties of different Cu-SSZ-13 and Cu-S-1 catalysts.

| Sample | Cu (wt.%) | Si/Al | Micropore area ($m^2/g$)[a] | Pore size(nm)[b] |
|---|---|---|---|---|
| Cu-SSZ-13(fresh) | 2.5 | 8.8 | 463 | 0.50 |
| Cu-SSZ-13(aged 12h) | 2.5 | 8.8 | 152 | 0.55 |
| Cu-S-1(fresh) | 2.2 | 8.8 | 391 | 0.51 |
| Cu-S-1(aged 12h) | 2.2 | 8.8 | 327 | 0.54 |

a Determined by the *t*-plot approach.
b Calculated by the H-K model.

results that isolated $Cu^{2+}$ species initially located in SSZ-13 framework were aggregated into large CuO particles during hydrothermal aging. Chemical properties of CuO species was completely different to the isolated $Cu^{2+}$ ions in the zeolite structure, which reduces SCR activities.[21] The XRD results in conjunction with the TEM results suggest the occurrence of two deactivation in Cu-CHA catalysts: the collapse of the SSZ-13 framework and CuO agglomeration, as has been discussed elsewhere.[22]

### 3.3 The influence of AHFS treatment time

The data thus far presented indicate that AHFS treatment clearly stabilizes Cu-SSZ-13 catalysts, but it remains to be determined whether additional AHFS treatment time would further increase this effect. To study this matter, Cu-SSZ-13 catalysts were treated with the same concentration of AHFS solution for different times.

The XRD results of the Cu-SSZ-13 catalysts obtained with different AHFS treatment times are shown in Fig. 4. The characteristic peaks of all the catalysts considered are related to the CHA phase, but the relative peak intensities are different. The crystal structures of the Cu-S-0.5 and Cu-S-1 catalysts were very stable after AHFS treatment, i.e., the relative intensities of the diffraction peaks were consistent with the untreated Cu-SSZ-13 catalyst. The peak intensities of Cu-S-2 at $2\theta$ values of 20.7° and 30.7° decreased slightly, whereas the other peak intensities were stable. However, the diffraction peak intensities of the Cu-S-4 catalyst were weaker than those of the other catalysts. This indicates that a prolonged AHFS treatment time has a harmful effect on the crystallinity of the samples.

The physicochemical properties of Cu-SSZ-13 catalysts prepared with different AHFS treatment times are listed in Table 1. As the period of AHFS treatment increased from 0.5 to 4 h, the Cu content of the catalysts decreased from 2.4% to 1.0%. This was caused by the exchange of $Cu^{2+}$ in the Cu-SSZ-13 catalyst with $NH_4^+$ ions derived from AHFS hydrolysis. As the increment of ion exchange time, increase of ion exchange level was accompanied by decrease of Cu content of the catalyst. Other research has indicated that AFHS treatment leads to a dealumination of the Cu-SSZ-13 framework. The Si/Al ratios of Cu-S-0.5 and Cu-S-1 remain unchanged, which suggests that almost all of the extracted aluminum atoms remain in pores of SSZ-13 framework.[23] However, the Si/Al ratios of Cu-S-2 and Cu-S-4 increased slightly because the AHFS treatment causes the removal of some Al atoms from the catalysts for treatment in excess of 2 h. Meanwhile, the micropore surface area of the modified Cu-SSZ-13 catalysts decreased with increasing AHFS treatment time. In addition, the pore size increased with increasing AHFS treatment.

We next measured the effects of AHFS treatment time on SCR performance. Fig. 5 shows the SCR performance of modified Cu-SSZ-13 catalysts with different AHFS treatment times. The NO conversion of the Cu-S-0.5 catalyst is similar to that of the Cu-S-1 catalyst because of their similar physicochemical parameters (Table 1). However, the NO conversion of the Cu-S-2 catalyst at low temperatures (< 200 °C) is slightly reduced relative to those of Cu-S-0.5 and Cu-S-1, while NO conversion at temperatures greater than 500 °C was increased, and was observed to be 70% at 550 °C. These results are consistent with previous findings of Cu-SSZ-13 with different Cu contents.[24, 25] While the Cu contents of the Cu-S-1 and Cu-S-2 catalysts were different, their crystallinities relative to the untreated Cu-SSZ-13 catalyst were well maintained. This indicates that the observed variations in the SCR activities are the result of variations in the Cu content of the catalysts. However, the NO conversion of Cu-S-4 was reduced over the entire temperature range

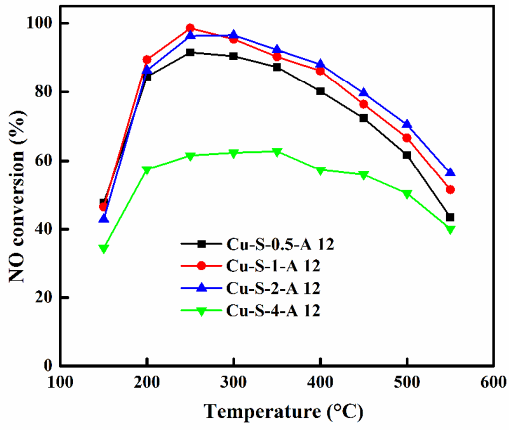

**Fig. 6** SCR performance for Cu-SSZ-13 catalysts with different AHFS treatment time after hydrothermal aging at 850 °C for 12 h.

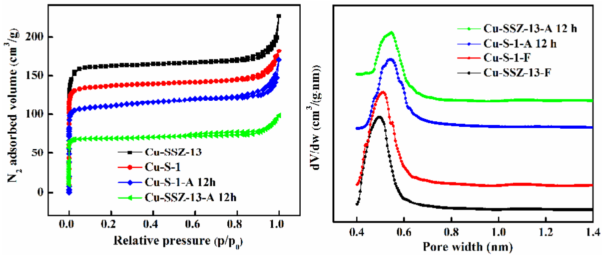

**Fig. 7** SCR performance for Cu-SSZ-13 catalysts with different AHFS treatment time after hydrothermal aging at 850 °C for 12 h.

considered, and the maximum NO conversion was about 75%, which was caused by both low Cu content and collapse of the CHA structure.

To understand the effects of hydrothermal aging on the NO conversion of modified Cu-SSZ-13 catalysts, all the catalysts were aged for 12 h, and the SCR activities are shown in Fig. 6. After hydrothermal aging, the medium temperature SCR activity (200–400 °C) was slightly reduced for all the catalysts considered, while NO conversion at temperatures less than 200 °C and greater than 400 °C decreased more significantly. Cu-S-1 demonstrated the best NO conversion performance at temperatures less than 400 °C. When the temperature was higher than 400 °C, NO conversion of Cu-S-2 was better than that of Cu-S-1. The catalytic performance of Cu-S-4 decreased over the entire temperature range after hydrothermal aging. For example, the maximum NO conversion was observed to be 63% at 350 °C, corresponding to a 10% reduction compared with the unaged catalyst. After hydrothermal aging, the catalytic activity of Cu-S-0.5 was lower than Cu-S-1, but it was still better than the untreated Cu-SSZ-13 catalyst.

### 3.4 Physical effect of AHFS treatment on the Cu-SSZ-13 catalyst

Figure 7 shows the N$_2$ adsorption-desorption isotherms and pore size distributions of the Cu-SSZ-13 and Cu-S-1 catalysts before and after hydrothermal aging. Table 2 summarizes the Cu contents, Si/Al ratios, micropore areas, and pore sizes of the untreated Cu-SSZ-13 and Cu-S-1 catalysts before and after hydrothermal aging for 12 h. It shows that the isotherms were all of type I, indicating that all the samples possessed microporous structure. The Cu content of the untreated Cu-SSZ-13 catalyst was greater than that of Cu-S-1, but the Si/Al ratios were equivalent. The elemental contents of untreated Cu-SSZ-13 and Cu-S-1 did not change after hydrothermal aging. After hydrothermal aging, the micropore areas of Cu-S-1 and untreated Cu-SSZ-13 decreased by 16.4% and 67.2% (i.e., from 391 and 463 m$^2$/g to 327 and 152 m$^2$/g), respectively. This indicates that greater damage occurred to the untreated Cu-SSZ-13 catalyst framework than to the Cu-S-1 framework during hydrothermal aging. After hydrothermal aging, the pore diameters of Cu-S-1 and untreated Cu-SSZ-13 increased from 0.51 and 0.50 nm to 0.54 and 0.55 nm, respectively.

The effects of hydrothermal aging on Si atoms and Al atoms in the Cu-S-1 and untreated Cu-SSZ-13 catalyst frameworks was investigated, the catalysts before and after hydrothermal aging were measured by solid-state NMR. As shown in Fig. 8a, the $^{27}$Al NMR spectra demonstrated that both fresh and aged Cu-S-1 and untreated Cu-SSZ-13 catalysts had a resonance peak at a chemical shift of 57 ppm, which was attributed to $^{27}$Al of the zeolite framework in tetrahedral coordination. For the Cu-S-1 catalyst, a peak appears at a chemical shift of around 18 ppm, which could be related to $^{27}$Al in octahedral coordination. This result indicates that extracted Al atoms remain in the pores as $(AlF_6)^{3-}$ after AHFS treatment. Meanwhile, the intensity of the peak at 57 ppm for the unaged Cu-S-1 catalyst decreased slightly relative to that of the initial untreated Cu-SSZ-13 catalyst, which was probably influenced by steric hindrance and AHFS treatment time, AHFS treatment had an effect only on a portion of the framework Al. After hydrothermal aging, the peak at 57 ppm becomes reduced for both Cu-S-1 and untreated Cu-SSZ-13 catalysts, which illustrated that dealuminization was occurred in framework of the catalysts during hydrothermal aging. Meanwhile, a new peak of both aged Cu-S-1 and untreated Cu-SSZ-13 catalysts appears a weak peak at around 0 ppm, which are considered as extra-framework $^{27}$Al in octahedral coordination, signifying that $^{27}$Al in the zeolite framework in tetrahedral coordination were transformed into octahedral aluminum upon dealumination under the influence of hydrothermal aging. When compared to the Cu-S-1 catalyst, the untreated Cu-SSZ-13 catalyst showed more obvious Al loss during aging, and more $^{27}$Al peaks in tetrahedral coordination were found to be reduced under the influence of aging, which indicates that the damage to Al in the untreated Cu-SSZ-13 framework was more serious during hydrothermal aging.

Fig. 8b displays the solid-state $^{29}$Si NMR spectra obtained from

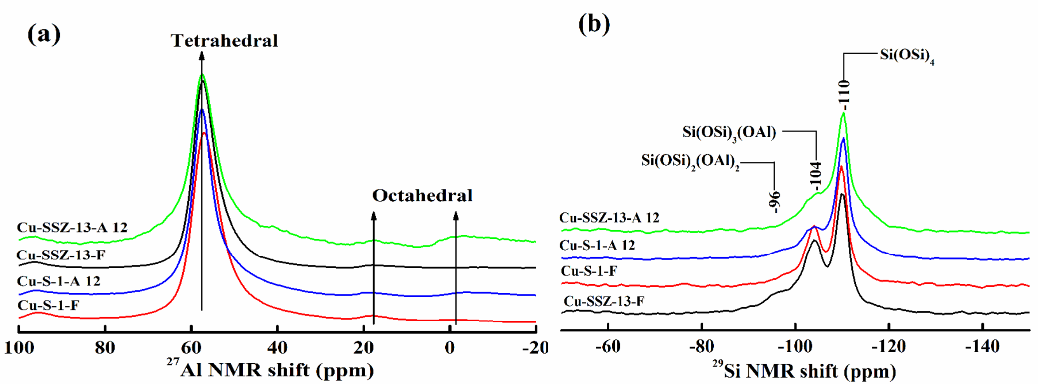

**Fig. 8** Solid state $^{27}$Al (a) and $^{29}$Si (b) NMR spectra of Cu-SSZ-13 and Cu-S-1 catalysts before and after aging.

the Cu-S-1 and untreated Cu-SSZ-13 catalysts before and after hydrothermal aging. The $^{29}$Si NMR spectra of both catalysts showed two peaks at −104 ppm and −110 ppm before and after hydrothermal aging, which were induced by the $Si(OSi)_3(OAl)$ and $Si(OSi)_4$ structures of the SSZ-13 zeolites, respectively. However, peaks owing to the $Si(OSi)_2(OAl)_2$ structure at a chemical shift of −96 ppm appeared only in the initial untreated Cu-SSZ-13 catalyst. Both hydrothermal aging and AHFS treatment result in the disappearance of the $Si(OSi)_2(OAl)_2$ peak. However, the reasons for this disappearance differ. The loss of the $Si(OSi)_2(OAl)_2$ structure by aging and AHFS treatment indicates that this structure is less stable than the $Si(OSi)_3(OAl)$ and $Si(OSi)_4$ structures. Hydrothermal aging leads $Si(OSi)_2(OAl)_2$ and $Si(OSi)_3(OAl)$ structures to dealuminate resulted in structural collapse. On the other hand, AHFS treatment of the Cu-SSZ-13 catalyst induces Al from the $Si(OSi)_2(OAl)_2$ structure to be replaced by Si to form the more stable $Si(OSi)_3(OAl)$ and $Si(OSi)_4$ structures, thus improving the hydrothermal stability of the Cu-SSZ-13 catalyst.

Fig. 9 shows vacuum FT-IR spectra for the initial untreated Cu-SSZ-13, Cu-S-1 and Cu-S-4 catalysts. After AHFS treatment, the absorption peak intensities of the $OH^-$ group at a wavenumber of around 3,400 $cm^{-1}$ and 3650 $cm^{-1}$ significantly decreased and become weaker with the increase of treatment time, which indicates that the Si-OH content of the untreated Cu-SSZ-13 catalyst decreased after AHFS treatment. The main absorption peaks corresponding to Si-O and Si-F bonds are at wavenumbers of 1,075–1,090 and 930 $cm^{-1}$, respectively. The Si-F bond absorption peak intensity for Cu-S-1 was weak, and could not be directly observed owing to interference from the strong Si-O peak nearby. As shown in Fig. 9, compared with Cu-SSZ-13, the Raman spectra of the Cu-S-1 and Cu-S-4 catalysts exhibit a new band centered at 950 $cm^{-1}$. The new band of Cu-S-1 catalyst which show the best catalytic activity was too weak and unable to identify. When treatment time was extended to 4 h, the Raman spectra of Cu-S-4 catalyst exhibit a more obvious band centered at 950 $cm^{-1}$. This new band is attributed to the vibration of Si-F according to a previous study.[26] This indicates that the $OH^-$ ion in surface Si-OH groups could be exchanged with $F^-$ ions from the decomposition of AHFS to form a hydrophobic surface, which can improve hydrothermal stability and more $OH^-$ ions of surface Si-OH groups were exchanged with $F^-$ ions with the increase of treatment time. Xu et al. used $^{19}$F NMR confirmed this exchange was occurred in an AlMCM-41 mesoporous material.[27] Because the binding energy of Si-F bonds is greater than that of Si-O bonds, it is more difficult for the Si-F bond to be broken. The hydrothermal stability of the catalyst can therefore be improved by the formation of these Si-F bonds.

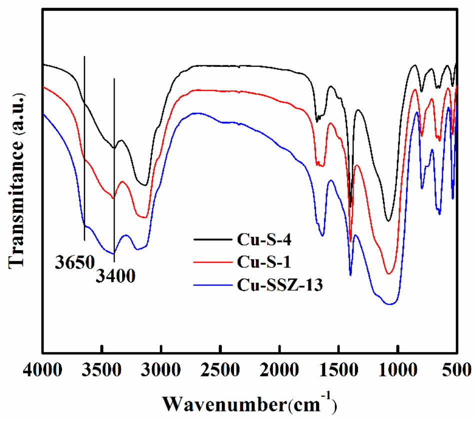

**Fig. 9** Vacuum FT-IR spectra of Cu-SSZ-13, Cu-S-1 and Cu-S-4 catalysts.

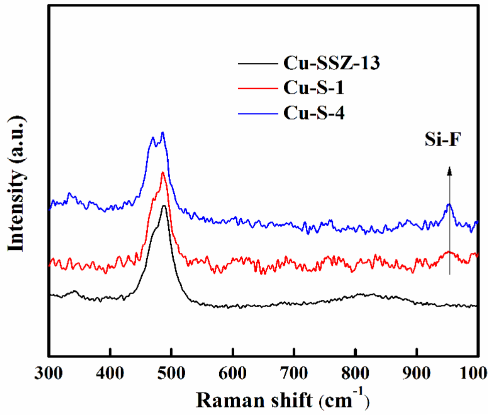

**Fig. 10** Raman spectra of Cu-SSZ-13, Cu-S-1 and Cu-S-4 catalysts.

## 4. Conclusions

The results indicate that hydrothermal aging at 850 °C for 12 h resulted in a significant reduction in the SCR performance of the Cu-SSZ-13 catalyst, which was accompanied by a significant loss in crystallinity and reduction in the number of active Cu sites. On the other hand, the AHFS-treated Cu-S-1catalyst suffered little loss in activity under equivalent aging conditions. This was explained by the AHFS treatment leading to the replacement of Al from the $Si(OSi)_2(OAl)_2$ structure with Si to form the more stable $Si(OSi)_3(OAl)$ and $Si(OSi)_4$ structures. Meanwhile, the $OH^-$ ions of the surface Si-OH groups could be exchanged with $F^-$ ions from the decomposition of AHFS to form a hydrophobic surface, which can also improve the hydrothermal stability. In addition, it was determined that an excessive AHFS treatment time damages the structure and catalytic performance of Cu-SSZ-13. Taken together, the results suggest that AHFS treatment is simple and does not alter the chemical properties and catalytic activity of Cu-SSZ-13 catalysts.

## Acknowledgements

The authors acknowledge the financial support of the Project Funded by the Priority Academic Program Development of Jiangsu Higher Education Institutions (PAPD) and the National Science Foundations of China (21101017).

Furthermore, the authors thank L. Sun (Nanjing University) for assistance in performing vacuum Fourier infrared.

## References

1. J. Kašpar, P. Fornasiero and N. Hickey, *Cataly. Today*, 2003, **77**, 419–449.
2. Fritza and V. Pitchon, *Appl. Catal. B*, 1997, **13**, 1–25.
3. M. V. Twigg, *Catal. Today*, 2011, **163**, 33–41.
4. T. J. Wang, S. W. Baek, H. J. Kwon, Y. J. Kim, I. -S. Nam, M. -S. Cha and G. K. Yeo, *Ind. Eng. Chem. Res.*, 2011, **50**, 2850–2864.
5. M. Iwamoto and H. Hamada, *Catal. Today*, 1991, **10**, 57–71.
6. M. Moliner, C. Franch, E. Palomares, M. Grill and A. Corma, *Chem. Commun.*, 2012, **48**, 8264–8266.
7. K. C. C. Kharas, H. J. Robota and D. J. Liu, *Appl. Catal. B*, 1993, **2**, 225–237.
8. S. A. Gomez, A. Campero, A. Martinez-Hernandez and G. A. Fuentes, *Appl. Catal. A*, 2000, **197**, 157–164.
9. J. H. Kwak, D. Tran, S. D. Burton, J. Szanyi, J. H. Lee and C. H. F. Peden, *J. Catal.*, 2012, **287**, 203–209.
10. D. Wang, Y. Jangjou, Y. Liu, M. K. Sharma, J. Y. Luo, J. H. Li, K. Kamasamudram and W. S. Epling, *Appl. Catal. B*, 2015, **165**, 438–445.
11. D. W. Fickel and R. F. Lobo, *J. Phys. Chem. C*, 2010, **114**, 1633–1640.
12. L. J. Xie, F. D. Liu, L. M. Ren, X. Y. Shi, F. S. Xiao, and H. He, *Environ. Sci. Technol.*, **2014**, 48, 566−572.
13. D. W. Fickel, E. D’Addio, J. A. Lauterbach and R. F. Lobo, *Appl. Catal. B*, 2011, **102**, 441–448.
14. S. J. Schmieg, S. H. Oh, C. H. Kim, D. B. Brown, J. H. Lee, C. H. F. Peden and D. H. Kim, *Catal. Today*, 2012, **184**, 252–261.
15. Y. J. Kim, J. K. Lee, K. M. Min, S. B. Hong, I. S. Nam and B. K. Cho, *J. Catal.*, 2014, **311**, 447–457.
16. H. Sun, Q. H. Tang, Y. Du, X. B. Liu, Y. Chen and Y. H. Yang, *J. Colloid. Interf. Sci.*, 2009, **333**, 317–323.
17. J. W. Wei, J. J. Shi, H. Pan, Q. F. Su, J.B. Zhu and Y. Shi, *Micropor. Mesopor. Mater.*, 2009, **117**, 596–602.
18. S. I. Zones, US Patent 4544538, 1985.
19. J. C. Wang, Z. L. Peng, Y. Chen, W. R. Bao, L. P. Chang and G. Feng, *Chem. Eng. J.* 2015, **263**, 9–19.
20. L. Ma, Y. Cheng ,G. Cavataio, R. W. McCabe, L. X. Fu and J. H. Li, *Chem. Eng. J.* 2013, **225**, 323–330.
21. J. Y. Yan, G. D. Lei, W. M. H. Sachtler and H. H. Kung, *J. Catal.*, 1996, **161**, 43–54.
22. J. C. Wang, Z. L. Peng, Y. Chen, H. Qiao, L. N. Han, W. R. Bao, L. P. Chang, G. Feng and W. Liu, *RSC Adv.*, 2014, **4**, 42403–42411.
23. P. Cañizares and A. Carrero, *Appl. Catal. A*, 2003, **248**, 227–237.
24. J. H. Kwak, D. Tran, J. Szanyi, C. H. F. Peden and J. H. Lee, *Catal. Lett.* 2012, **142**, 295–301.
25. Y. Zhang, H. N. Wang and R. Y. Chen, *Acta Phys.-Chim. Sin.*, 2015, **31(2)**, 329–336.
26. G. D. Chen, L. Z. Wang, J. Y. Lei and J. L. Zhang, *Micropor. Mesopor. Mater.*, 2009, **124**, 204–209.
27. M. Xu, W. Wang, M. Seiler, A. Buchholz and M. Hunger, *J. Phys. Chem. B*, 2002, **106**, 3202–3208.